ELSEVIER

Journal of Nuclear Materials 300 (2002) 118–126

journal of nuclear materials

www.elsevier.com/locate/jnucmat

A Raman study of the nanocrystallite size effect on the pressure–temperature phase diagram of zirconia grown by zirconium-based alloys oxidation

P. Bouvier [a], J. Godlewski [b], G. Lucazeau [a,*]

[a] *Laboratoire d'Electrochimie et de Physico-chimie des Matériaux et des Interfaces (LEPMI), 1130 rue de la piscine, BP 75, 38402 St Martin d'Hères cedex, France*

[b] *CEA Cadarache DEN/DEC/S3CC/LCG, BP 1, 13108 St Paul-lez-Durance, France*

Received 24 September 2001; accepted 21 November 2001

Abstract

The pressure–temperature phase diagrams of different zirconia samples prepared by oxidation of Zircaloy-4 and Zr–1%Nb–0.12O alloys were monitored by Raman spectrometry from 0.1 MPa to 12 GPa and from 300 to 640 K. These new diagrams show that the monoclinic–tetragonal equilibrium line is strongly downshifted in temperature compared to literature measurements performed on usual polycrystalline zirconia. In addition, the monoclinic–orthorhombic equilibrium line is slightly shifted to higher pressure (i.e. 6 GPa). The crystallite sizes smaller than 30 nm, are thought to be responsible for these equilibrium line displacements. The tetragonal phase obtained in temperature under high pressure can be quenched at room temperature, if the pressure is maintained, and it is destabilised and transforms completely into monoclinic phase if the pressure is released. These results confirm that coupled effects of stress, temperature and nanosized grain are responsible for the formation of the tetragonal phase near the metal/oxide interface during the oxidation of zirconium-based alloys.

1. Introduction

It is now well admitted that the oxide layer, which develops during zirconium alloy corrosion process in pressurised autoclave at 630 K, consists in a mixture of tetragonal and monoclinic zirconia polymorphs. It was shown from Raman measurements [1–3], that the tetragonal form is preferentially located close to the metal/oxide interface. The oxide films can be divided into two sublayers. The first one, close to the metal/oxide interface, plays the role of barrier layer for the oxidising species and is composed of a mixture of tetragonal and monoclinic zirconia. The second one corresponds to the outer part porous layer and is only composed of monoclinic zirconia. This description is also supported by electrochemical impedance spectrometry characterisations performed either in liquid solution [4,5] or in gaseous atmosphere [6].

The mechanism of stabilisation of the tetragonal form in a thin layer close to the metal/oxide interface is however still under discussion and is of considerable interest to understand the oxidisation mechanism. Crystallite size effect, point defects and intrinsic stresses generated during the growth process are always listed as possible stabilising parameters.

(i) The crystallite size effect has been studied in undoped zirconia powders either at room temperature for increasing annealing treatments [7,8] or at high pressure [9]. It has been concluded that ideal crystallites smaller than 25–30 nm are stable in a broad pressure–temperature (P–T) range, in agreement with early Garvie's conclusions based on surface energy considerations [10]. We shall show in the last section that it is possible

* Corresponding author. Tel.: +33-4 76 82 65 00; fax: +33-4 76 82 66 30.

E-mail address: guy.lucazeau@lepmi.inpg.fr (G. Lucazeau).

0022-3115/02/$ - see front matter
PII: S0022-3115(01)00756-5

to reproduce the temperature downshift of the tetragonal–monoclinic transformation of nanocrystalline zirconia. Preliminary results were presented in [11,12]. In oxidation film, X-ray diffraction (XRD) [7,13] and transmission electronic microscope (TEM) data [14–16] agree to measure a mean crystallite size lower than the above critical size value, with no appreciable size variation inside the whole film. Thus the size effect is not sufficient by itself to explain, either the presence of a thin layer of tetragonal zirconia close to the metal/oxide interface nor its disappearance when the underlying metal is removed (as shown in Ref. [3]).

(ii) The effect of dopants, like trivalent Fe^{3+} [17] or tetravalent Sn^{4+} [18,19] could contribute to a tetragonal stabilisation in the vicinity of $Zr(Fe,Cr)_2$ precipitates as suggested in [20,21]. On the contrary, charges compensating pentavalent Nb^{5+} that are found in Zr1%Nb alloy are believed to reduce the tetragonal stability [22]. In oxidation films, dopant amount is low and cannot be sufficient to explain the stabilisation of the tetragonal form, whereas it can play a major role in the destabilisation process (see Ref. [23]).

(iii) The internal compressive stresses generated during the growth process remain as another possible candidate for the tetragonal phase stabilisation [1,3,15]. In addition, these stresses are thought to be larger at the metal/oxide interface in connection with the observation of a maximum in the proportion of tetragonal phase [1,3]. Stresses measured by XRD or by Raman spectroscopy are close to 1.5–2 GPa. These values are in good agreement with numerical Parise's calculations [24]. Notice that for a pressure of 2 GPa, following thermodynamic literature data [25,26] the tetragonal form can be obtained from a pure microcrystallized zirconia above 850 K, i.e. at a temperature larger than that fixed for obtaining the present samples.

In the present study, different samples of zirconia, representative of the oxides formed in pressurised water, were submitted to a combined effect of pressure and temperature. The study was confined to the temperature and pressure ranges below 12 GPa and 650 K. It will be shown that the nanosize of crystallites induce large displacements of transition lines in the P–T phase diagram of zirconia and that the tetragonal phase is stable towards temperature, provided the pressure is maintained. These conclusions will be related to previous observations made on taper cross-sections and to recent [11,27] in situ Raman monitoring of zirconium alloys oxidation.

2. Experimental Part

Zircaloy-4 (1.3%Sn–0.2%Fe–0.1%Cr–0.13%O_2) and Zr–1%Nb–0.12%O_2 alloys were oxidised in water at 630 K and 186 bars for two different lithium and boron contents (10 ppm Li and 650 ppm B, 70 ppm Li). These alloys are noted Zy4 and ZrNb in the following and are followed by a number corresponding to the Li content in ppm of the oxidising water medium (see Table 1). Two pre-transition samples of ZrNb-70 and ZrNb-10 and a post-transition sample of Zy4-10 have been investigated. The oxidation curves of ZrNb and Zy4 alloys are presented in Fig. 1. Structural characteristics of oxide films, such as thickness and crystallite average size deduced from TEM measurements, are reported in Table 1. Zirconia scales were detached from the substrate by dissolution of metal in $HF/HNO_3/H_2O$ mixture. After such a process, the oxide film contains only monoclinic form, the transformation of the tetragonal phase being related to the relaxation of stresses, which were present at the metal oxide interface. A commercial powder (Tosoh) of monoclinic zirconia was also used as a reference. The average crystallite size was found close to 35 nm from measurements of profiles of X-ray diffraction lines based on the Scherrer formula: $D = 0.9\lambda/\beta\cos\theta$, where D is the crystallite size, λ the wavelength, β the corrected full width at half maximum using high purity silicon and θ the diffraction angle.

Raman spectra were obtained using an XY Dilor multichannel spectrometer equipped with a CCD detector. The 514.53 nm line of an Argon ion laser was used as the excitation source in a back scattering geometry. After focusing with a $\times$20-magnification

Table 1
Characteristic of oxidised samples

Sample	Alloy	Oxidation time (day)	Oxidation conditions	Thickness (μm)	Crystallite sizes (nm)
ZrNb-70	Zr–1%Nb	90	70 ppm Li	2.48	20–50[a]
ZrNb-10	Zr–1%Nb	250	10 ppm Li 650 ppm B	3.47	20–50[a]
Zy4-10	Zircaloy-4	250	10 ppm Li 650 ppm B	5.51	15–30[a]
Tosoh®	Pure ZrO_2				30–35[b]

[a] Correspond to TEM observations.
[b] States for XRD measurements using Scherrer's formula.

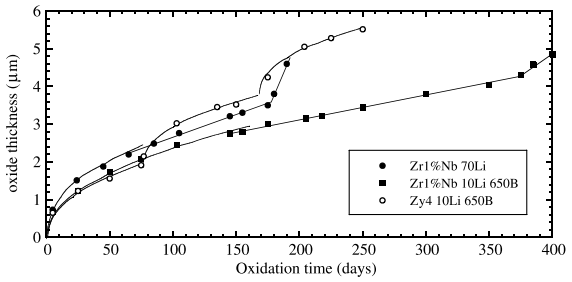

Fig. 1. Oxidation curves of Zr-1%Nb and Zy4 zirconium alloys in two different water chemistry. Temperature was 630 K and pressure was 18 MPa. Lithium and Bore contents in ppm are indicated on the figure and in Table 1.

objective, the laser spot was about 2 μm in diameter. All spectra were decomposed into lorentzian components using the Jandel's PEAKFIT software.

Samples were studied under isostatic high pressure and high temperature in a diamond anvil cell (DAC) equipped with a heating gasket developed at CEA Valduc [28]. The pressure-transmitting medium was argon compressed at 0.25 GPa. The pressure and the temperature were measured from the fluorescence lines of grains of ruby (Al_2O_3:Cr^{3+}) [29] and strontium borate (SrB_4O_7:Sm^{2+}) respectively. These probes were distributed all around the samples in order to check that no gradients of pressure and temperature were detectable. Experimental uncertainties on pressure and temperature were equal to ±0.1 GPa and ±5 K respectively. Three zirconia samples were placed in the same DAC and were investigated in sequence for each pressure and temperature change.

Non-isostatic measurements have also been performed in a DAC without any pressure-transmitting medium by introducing directly in the gasket, zirconia powders obtained by grinding oxide scales. In that case an argon laser was used to heat the samples. The temperature was deduced from Stokes and anti-Stokes Raman lines intensities, using the following formula:

$$I_{\mathrm{Stokes}}/I_{\mathrm{anti-Stokes}} = \left\{(\nu_o - \nu_n)^4/(\nu_o + \nu_n)^4\right\}\exp(h\nu_n/kT),$$

where ν_o is the wave number of the excitation line and ν_n that of a Raman line; h and k are the Planck and Boltzmann constants respectively. A reasonable estimation of temperature is obtained in the 400–800 K range, for example, an incident power of 1.2 W induces a local (4 μm^2) temperature raise of 500 ± 50 K. The pressure was measured from fluorescence of ruby.

The reference monoclinic (Tosoh) zirconia was also studied in a DAC at 300 K using an ethanol–methanol–water mixture as a pressure-transmitting medium.

3. Results and evidence of phase transition

3.1. Isostatic high pressure–high temperature measurements

The P–T couples in which Raman spectra of the three samples have been recorded are plotted in Fig. 2. For each of these P–T couples, the Raman spectra of the three samples have been recorded. Because of the deformation of iron gaskets upon heating, pure isothermal or isobaric displacements could not be achieved. The high pressure measurements performed at room temperature on the reference Tosoh pure zirconia powder are represented by open triangles.

The stability domains of monoclinic, tetragonal and orthorhombic polymorphs of usual microcrystalline zirconia as given in the literature [25,26] are defined by dashed-dotted line on Fig. 2. Continuous lines and dotted lines represent domains of existence of these forms for zirconia resulting from oxidation of Zr–1%Nb and Zircaloy-4 alloys respectively. These lines were estimated from the spectra recorded in each P–T point and

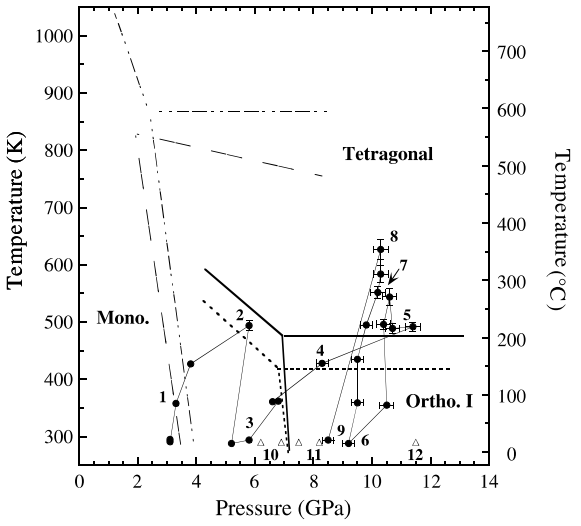

Fig. 2. P–T phase diagram of zirconia. The different P–T couples that were explored under hydrostatic high pressure and high temperature conditions are plotted. At each P–T couple (●), a Raman spectrum has been recorded on zirconia resulting from oxidisation of Zr–1%Nb-10, Zr–1%Nb-70 and Zy4-10 alloys. The open triangles correspond to a high-pressure experiment performed on a Tosoh reference monoclinic zirconia. The monoclinic–tetragonal (M–T), monoclinic–orthorhombic (M–O_I) and orthorhombic–tetragonal (O_I–T) line boundaries of microcrystalline zirconia are reported in dot-dashed and double dot-dashed lines using Refs. [25,26] respectively. The approximative M–T, M–O_I and O_I–T line boundaries of nanocrystalline Zr–1%Nb and Zy-4 grown zirconias are reported in plain and dashed lines respectively.

used for monitoring the appearance of the different polymorphs. When Raman bands of a new phase appear with about 10% of their intrinsic intensity, we have considered that a transition line is being crossed. A coexistence of phases is observed for most of the points, this can be due to the first order nature of the transition and to the crystallite size dispersion. For these reasons, the uncertainty in the positioning of transition lines can reach 50 K.

3.1.1. Monoclinic–orthorhombic transition

The Tosoh reference monoclinic zirconia sample has been studied up to 11.5 GPa. The Raman spectra represented in Fig. 3 correspond to the monoclinic form at 6.2 GPa, (spectrum 3a), the orthorhombic form O_I (Pbca, D_{2h}^{15}) at 11.5 GPa, (spectrum 3c) and a mixture of these phases at the intermediate pressure 8.8 GPa (spectrum 3b).

Fig. 4 represents a selection of six spectra measured on the ZrNb-70 sample for the *P–T* couples corresponding to points 1 to 6 in the *P–T* diagram of Fig. 2. Spectra (1)–(3) correspond to a monoclinic zirconia sample in which the main Raman lines are shifted under the combined effect of pressure and temperature. The monoclinic line at 100 cm^{-1} is particularly sensitive toward pressure as reported in Ref. [30,31]. The monoclinic line at 160 cm^{-1} has disappeared in spectrum (4) while two new weak lines at 150 and 170 cm^{-1} (marked with a black circle) are present. These spectral features are the indication that the orthorhombic O_I polymorph is being formed. The doublet at 180–208 cm^{-1}, very similar to the characteristic monoclinic doublet at 190 and 200 cm^{-1} is actually attributed to the orthorhombic

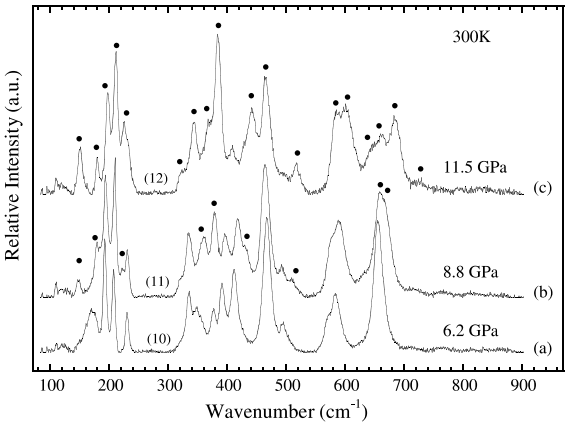

Fig. 3. Selection of Raman spectra recorded at room temperature on a Tosoh monoclinic zirconia for increasing pressure from (a) 6.2 GPa, (b) 8.8 GPa to (c) 11.5 GPa. The black circles in spectrum (b) indicate lines characteristic of the orthorhombic form. The spectrum (c) corresponds to pure orthorhombic (Pbca) phase. We report into bracket the number of the corresponding points in the *P–T* phase diagram of Fig. 2.

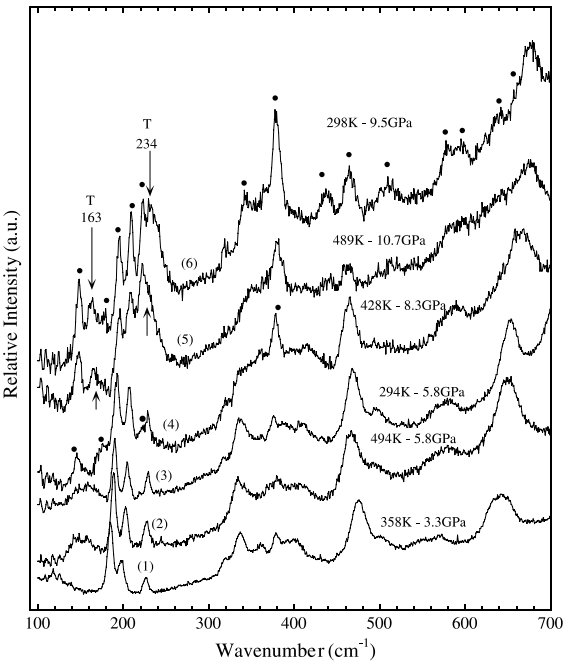

Fig. 4. Raman spectra recorded on Zr–1%Nb-70 zirconia for various temperature and pressure from (1) 358 K–3.3 GPa, (2) 494 K–5.8 GPa, (3) 294 K–5.8 GPa, (4) 428 K–8.3 GPa, (5) 489 K–10.7 GPa to (6) 298 K– 9.5 GPa. The number into brackets corresponds to special points in the *P–T* phase diagram of Fig. 2. Black circles indicate Raman lines associated with orthorhombic phase. Arrows indicate Raman lines associated with the tetragonal phase.

O_I phase [30,31]. All the monoclinic lines in the 300–400 cm^{-1} region have disappeared while the band at 465 cm^{-1} is quite similar to that belonging to the monoclinic structure, indicating that there is continuity in the eigen-modes through the phase transitions. The spectra obtained on the Tosoh reference sample at room temperature under increasing pressure illustrate the above remark. Thus, the M–O_I transition for these nanometric zirconia takes place between 6 and 8.4 GPa and in a temperature range comprised between 300 and 450 K. Non-isostatic data (see Fig. 7) obtained at 6.7 and 7.2 GPa at 300 K allow a better definition of the monoclinic–orthorhombic frontier. Finally it must be noted that at room temperature this frontier is displaced from 4 GPa, as represented by dashed lines in Fig. 2 [25,26], to 7 GPa in the Tosoh sample.

3.1.2. Orthorhombic–tetragonal transition

The spectrum (5), in Fig. 4, obtained at 489 K and 10.7 GPa, exhibits two new weak lines at 153 and 230 cm^{-1}. These lines correspond to the 150 and 260 cm^{-1} modes of the tetragonal form shifted by the pressure effect. These wave numbers after correction of the

Table 2
Temperature induced frequency shifts and Gruneisen parameters for two characteristic vibrational modes of a tetragonal 18 nm nanometric zirconia

Vibrational modes ν_i (cm^{-1})	Temperature 80–700 K		Pressure 0.1 MPa–10 GPa		Frequency shift $\Delta\nu$ (cm^{-1}) $\Delta\tau = 590\ K \rightarrow 300\ K$	
	$(d\nu/dT)_P$ (cm^{-1}/100 K)	γ_P	$(d\nu/dP)_T$ (cm^{-1}/GPa)	γ_T	At $P = 0.1$ MPa	At $P = 4.1$ GPa
150	−0.20(1)	+0.7	+1.75(1)	+2.2	+0.58(3)	+0.7(2)
260	−1.86(8)	+2.0	−3.59(4)	−2.5	+5.4(2)	+5.9(5)

$\gamma_P = -1/\beta\nu_i(d\nu/dT)_P$ where β is the thermal expansion coefficient. $\gamma_T = -1/\kappa\nu_i(d\nu/dP)_T$ where κ is the compressibility coefficient.

pressure effect are found close to those of tetragonal zirconia [32,33]. Gruneïsen coefficients of a nanocrystallised tetragonal zirconia of Table 2 [11], were used to check that the spectral behaviour of these lines were consistent with their expected shifts. This spectrum is thus characteristic of the mixture of orthorhombic and tetragonal polymorphs. The composition of these phases is not affected by a rapid temperature decrease down to 295 K while maintaining high pressure (point 9 in Fig. 2). The corresponding spectrum, which is presented in Fig. 5, contains the same bands of the tetragonal form, slightly shifted by the temperature decrease. This shows that the tetragonal form can be maintained at room temperature, provided that pressure is maintained.

In the same way, Fig. 6 shows that the destabilisation of the tetragonal form maintained in a metastable state under 9 GPa at 300 K, is achieved when the pressure is lowered to 3 GPa.

3.2. Non-isostatic high pressure measurements coupled with laser heating

Fig. 7 represents the P–T phase diagram of ZrO_2 along with the investigated P–T couples. In these experiments, the same samples were submitted to a non-isostatic pressure comprised between 1 and 7 GPa and in the 300–580 K temperature range. Notice that localised laser heating has allowed us to follow isobaric paths. Fig. 8 corresponds to the isobar line 4.1 GPa and represents Raman spectra measured on ZrNb-70 before heating (spectrum 8a), under laser heating (spectrum 8b) and after rapid return to 300 K (spectrum 8c).

From the results obtained on ZrNb-70, one can conclude that the monoclinic zirconia is transformed partly into its tetragonal form at 590 K and 4 GPa, without observing traces of orthorhombic phase. Raman spectra are characteristic of a mixture of tetragonal and monoclinic zirconia and are very similar to those measured on oxidised taper cross-sections [3]. In that case too, the tetragonal zirconia is not destabilised when temperature is decreased to 300 K while pressure is maintained.

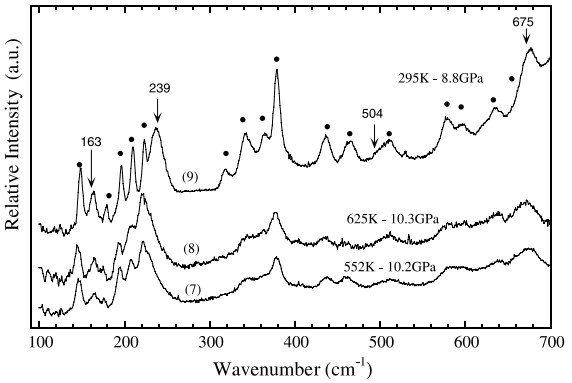

Fig. 5. Raman spectra recorded on Zr-1%Nb-70 sample for high temperature and nearly constant pressure from (7) 552 K–10.2 GPa, (8) 625 K–10.3 GPa to (9) 295 K–8.8 GPa. The numbers into brackets correspond to investigated P–T points in phase diagram of Fig. 2. Black circles indicate Raman lines of the orthorhombic phase. Arrows indicate Raman lines of the tetragonal phase with their wavenumber at 295 K– 8.8 GPa.

Under 4.1 GPa, the Raman lines, attributed to the tetragonal zirconia, shift from 153 to 153.7 cm^{-1} and from 255 to 261 cm^{-1} when temperature is decreased from 570 to 298 K. These shifts are close to those observed at atmospheric pressure (Table 2), by the same temperature shift [11]. Thus it can be concluded that thermal effects on wave numbers are nearly independent of the pressure, at least below 12 GPa. Fig. 9 represents a typical Stokes and anti-Stokes spectrum used for temperature measurements under laser heating.

4. Discussion

This section is devoted to a discussion on the new phase diagram relative to monoclinic–orthorhombic–tetragonal polymorphs of zirconia formed by oxidation of zirconium alloys. The conditions of metastability of the tetragonal form will be analysed.

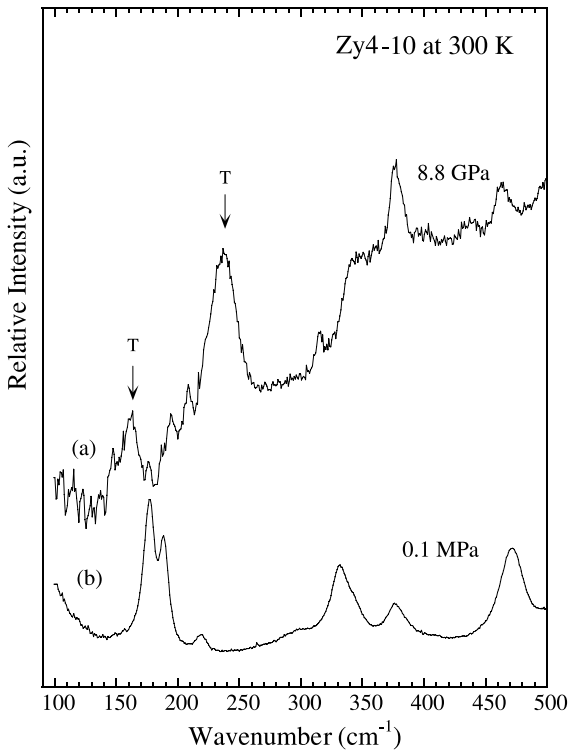

Fig. 6. (a) Raman spectrum recorded at 298 K, 8.8 GPa point (9) in the P–T diagram of Fig. 2 on Zy4-70 zirconia after a high pressure and high temperature cycle. (b) Raman spectrum recorded after a sudden pressure release. Arrows indicate Raman lines of the tetragonal phase.

4.1. Effect of crystallite size on the P–T diagram of zirconia formed on zirconium alloys

The phase diagram of these nanometric zirconia (Figs. 2 and 7) is quite different from that published by Bocquillon and Susse [25] or by Block et al. [26]. The existence domains of the different polymorphs are strongly displaced toward high pressure for the orthorhombic phase or low temperature for the tetragonal phase. These differences can be explained by an effect of crystallite nanosize. It is well known that the melting or transformation temperature depends on the radius of crystallites. The Gibbs–Thomson relationship [34] can be applied to determine the melting temperature of small crystals, where T is the melting temperature of a small crystal.

$$\frac{T - T_0}{T_0} = -\frac{2V_T}{\Delta H_{M\text{–}T}}\sigma\frac{1}{r}.$$

The transposition of this relationship to a solid–solid transformation is possible, provided an amorphous interface is present between the two solid phases [35,36]. The existence of at least a disordered monolayer separating two crystallites is a reasonable assumption for applying this relationship to the monoclinic–tetragonal polymorphic transformation. In a first step, only a qualitative representation of the effect of the size parameter on the phase transformations is studied. T is the transformation temperature of a monoclinic nanocrystallite into the tetragonal embedding form (playing the role of the surrounding liquid in the melting process). T_0

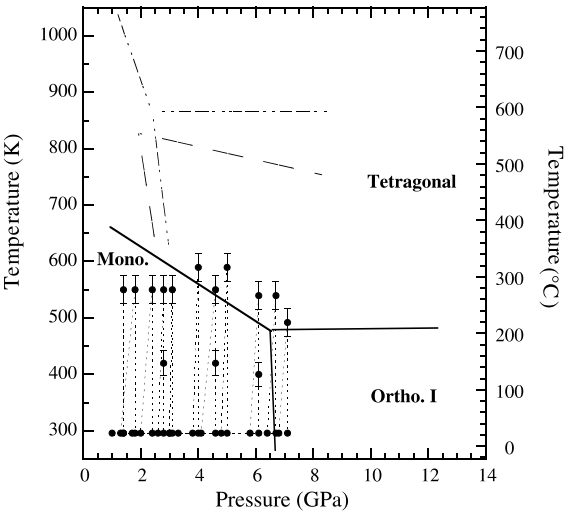

Fig. 7. Revisited P–T phase diagram of ZrNb-70 zirconia determined from non-isostatic high pressure experiment. The temperatures obtained by local laser heating of the sample are quoted on the figure. The M–T, M–O_I and O_I–T line boundaries of microcrystalline zirconia represented in dotted-dashed and double dot-dashed lines were drawn from Refs. [25,26] respectively. The M–T, M–O_I, O_I–T line boundaries of nanocrystalline Zr–1%Nb-70 zirconia are reported in plain lines.

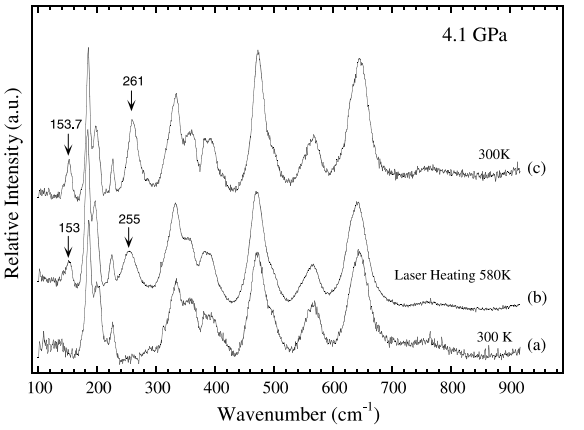

Fig. 8. Raman spectra recorded on ZrNb-70 zirconia under 4.1 GPa non-isostatic pressure, for increasing temperature from (a) 298 K, (b) 590 K to (c) 298 K using laser heating. The Raman lines of the tetragonal phase are indicated by arrow.

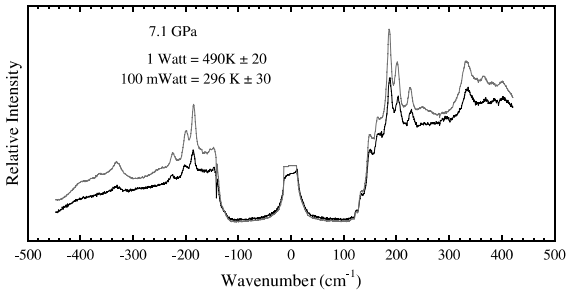

Fig. 9. Stokes and anti-stokes Raman spectra of a Zr-1%Nb sample heated by laser and submitted to a non-isostatic pressure of 7.1 GPa. The incident power used and the corresponding temperature are reported on the figure.

is the 1473 K transformation temperature for bulk crystal, $\Delta H_{M-T} = 5.93$ kJ mol^{-1} is the monoclinic–tetragonal transformation enthalpy, $V_T = 20$ cm^3 is the molar volume of tetragonal form, r is the radius of the crystallite, σ is the monoclinic–tetragonal interfacial energy. For a crystallite diameter of 7 nm ($r = 3.5$ nm in the above formula) and a $T - T_0$ downshift of 1400 °C (T is below 200 K) as measured for the transition temperature of 7 nm nanometric zirconia [37], one obtains a reasonable value for $\sigma = 0.5$ J m^{-2} [11] which validates the above model. Thus, in the case of crystallites ranging between 15 and 30 nm in diameter, one expects at room pressure that the transition temperature is about 773 K. A small increment of pressure (provided by compressive stresses close to the metal/oxide interface) is thus sufficient to stabilise the tetragonal form in the conditions of oxidation of zirconium alloys. In conclusion, the crystallites size parameter is able to explain the phase diagram changes, the coexistence of phases observed near transition lines being due to the distribution of crystallite sizes.

As already mentioned the monoclinic–orthorhombic transition takes place on a broad temperature range and is characterised by a hysteresis. This is explained, on the one hand, by the above mentioned dispersion of crystallites and, on the other hand, by the first order nature of the transition. Among the thermodynamic data the molar volume variation at the transition is reported equal to $\Delta V = -1.82$ cm^3 mol^{-1} [38].

The monoclinic–orthorhombic separation line deduced from our measurements presents a negative slope, in good agreement with that, $(\partial P/\partial T)_V = -9.1 \times 10^{-3}$ GPa K^{-1}, reported by Ohtaka et al. [38]. However, the frontier is found at about 7 GPa at 300 K, while it is reported between 3.5 and 4 GPa in Refs. [25,26,30,31], and at 6 GPa, for crystallites smaller than 30 nm [39]. It is found close to 9.5 GPa in Ref. [40] and to 10 GPa in [41] depending on the crystalline state, on the crystallite size and on the kinetic of pressure variation. The monoclinic–orthorhombic transition pressure increases when the crystallite size decreases, and the transition pressures measured on zirconia powders originating from oxidised Zircaloy and on the reference Tosoh zirconia are consistent with a crystallite size of a few 10 nm in agreement with that measured on these oxides.

If the crystallite nanosize plays a key role in the lowering of the tetragonal–monoclinic transformation temperature, it also contributes to induce frequency shifts. The vibrational modes of the tetragonal form measured at 280 and 454 cm^{-1} in oxidation films are shifted by comparison with pure 18 nm zirconia prepared by pyrosol technique, in which these modes are reported at 267 and 460 cm^{-1} respectively. Barberis et al. [42] attribute these shifts to a hyper tetragonal structural strain of oxygen lattice (without giving the origin of this strain). We think that these shifts can be explained simply by consideration of the phonon confinement model [43]. A reference to this model was made in Ref. [8] to explain the continuous increase of the mode from 267 to 279 cm^{-1}, when crystallites sizes decrease from 30 to 7 nm. The evolution of these modes cannot be correlated with a possible internal pressure to balance the surface tensile stress, because this internal stress would be small and it could not satisfy the positive shift of the 270 cm^{-1} mode.

Finally, considering the continuous and dotted lines in Fig. 2, the tetragonal form appears 50 °C lower when it is formed on Zy-4 than on Zr–1%Nb. This observation is consistent with the smaller size of crystallites generated for this alloy (Table 1).

4.2. Metastability of tetragonal zirconia

This property is illustrated by Fig. 6 which represents the spectra of a Zy4-10 sample obtained in its tetragonal form under isostatic conditions at 650 K, 10 GPa (point 8 in Fig. 2), returned to 300 K and maintained under a pressure of 8 GPa. The corresponding spectrum indicates that the sample is still in its tetragonal form. A decrease of temperature to 300 K is not sufficient to activate the transition, while a decrease of pressure leads to a complete transformation towards its monoclinic form. This observation is the proof that, after the oxidation process performed at 630 K, the return to room temperature of zirconia scales still adherent to underlying metal does not alter the repartition of tetragonal form in the film. On the contrary, the relaxation of stresses, which takes place when the underlying metal is dissolved in acids, destabilises the tetragonal form. This destabilisation has been reported in Ref. [3]. These observations constitute a further proof that the preparation of films as taper cross-sections does not perturb the mechanical equilibrium of the film.

Petigny et al. [44] have stated that the cooling process of oxidised films induces compressive stresses which would be dominant compared to internal ones generated during the growth of the film. In addition one could also

raise the question of their responsibility in the formation of tetragonal zirconia. Recent Raman in situ monitoring of the oxidation of Zr–Nb alloys at 633 K in water atmosphere has confirmed the formation of tetragonal form. This study has also demonstrated that the cooling process generates stresses of about 500 MPa quite insufficient for increasing the proportion of tetragonal zirconia generated during the growth of the oxide film and smaller than stresses measured at 630 K [11,27].

5. Conclusions

The *P–T* phase diagram of the different zirconia samples obtained by oxidation of Zircaloy-4 and Zr–1%Nb alloys in pressurized water for two compositions of Li and B is presented. The monoclinic–tetragonal transformation has been found to take place at a much lower temperature and pressure than those, which are expected, from the phase diagram of the pure microcrystalline zirconia. This result can be related to the nanostructure of the crystallites constituting oxidation scales. It has been shown that the tetragonal form maintained under a moderate pressure can be cooled down to room temperature without being destabilised. On the contrary any release of pressure induces the destabilisation of this form towards the initial monoclinic polymorph. These results validate the important role played by temperature, pressure and grain size, in the oxidation process and in the stabilisation of the tetragonal form at the metal/oxide interface. The small dependence of the *P–T* diagram with the nature of the alloy is likely due to the small variation in the average crystallise size from Zr1%Nb to Zy4 alloys. The effect of the composition of the oxidising medium on the thermoelastic properties of the oxides could not be evidenced.

Finally this study validates the results relative to the proportion of this phase in the oxidation films obtained from ex situ analysis conducted previously on taper cross section and that the cooling process of the oxide does not affect the proportion of the tetragonal form.

Acknowledgements

B. Sitaud and F.X. David from CEA Valduc are acknowledged for the loan of the heating diamond anvil cell and their contribution to the experiments. N. Rosman is also acknowledged for his participation in Raman measurements.

References

[1] J. Godlewski, J.P. Gros, M. Lambertin, J.F. Wadier, H. Weidinger, ASTM-STP 1132 (1991) 416.
[2] J. Godlewski, ASTM-STP 1245 (1994) 663.
[3] J. Godlewski, P. Bouvier, G. Lucazeau, L. Fayette, ASTM-STP 1354 (1998) 877.
[4] O. Gebhardt, A. Hermann, Electrochim. Acta 41 (1996) 1181.
[5] P. Barberis, A. Frichet, J. Nucl. Mater. 273 (1999) 182.
[6] J.J. Vermoyal, A. Frichet, L. Dessemond, A. Hammou, Electrochim. Acta 45 (1999) 1039.
[7] P. Barberis, J. Nucl. Mater. 226 (1995) 34.
[8] E. Djurado, P. Bouvier, G. Lucazeau, J. Solid State Chem. 149 (2000) 399.
[9] P. Bouvier, G. Lucazeau, J. Phys. Chem. Solids 61 (2000) 569.
[10] R.C. Garvie, J. Phys. Chem. 69 (1965) 1238.
[11] P.Bouvier, thèse de doctorat, INPG (2000).
[12] P. Bouvier, G. Lucazeau, Journées études transitions de phase, Montpellier, Mar. 2001.
[13] A.J.G. Maroto, R. Bordoni, M. Villegas, A.M. Olmedo, M.A. Blesa, A. Iglesias, P. Koenig, J. Nucl. Mater. 229 (1996) 79.
[14] F. Garzarolli, H. Siedel, R. Tricot, J.P. Gros, ASTM-STP 1132 (1991) 395.
[15] H.J. Beie, A. Mitwalsky, F. Garzarolli, H. Ruhmann, H.J. Sell, ASTM-STP 1245 (1994) 615.
[16] D. Pêcheur, J. Godlewski, P. Billot, J. Thomazet, ASTM-STP 1295 (1996) 94.
[17] P. Li, I.-W. Chen, J.E. Penner-Hahn, J. Am. Ceram. Soc. 77 (1994) 118.
[18] P. Li, I.-W. Chen, J.E. Penner-Hahn, J. Am. Ceram. Soc. 77 (1994) 1281.
[19] D.-J. Kim, J.-W. Jang, H.-L. Lee, J. Am. Ceram. Soc. 80 (1997) 1453.
[20] D. Pêcheur, F. Lefebvre, A.T. Motta, C. Lemaignan, D. Charquet, ASTM-STP 1245 (1994) 687.
[21] X. Iltis, F. Lefebvre, C. Lemaignan, J. Nucl. Mater. 224 (1995) 121.
[22] D.J. Kim, J. Am. Ceram. Soc. 73 (1990) 115.
[23] S. Lawson, J. Eur. Ceram. Soc. 15 (1995) 485.
[24] M. Parise, thèse de doctorat, ENS Mines de Paris, 1996.
[25] G. Bocquillon, C. Susse, Rev. Int. Hautes Tempér. Réfract. 6 (1969) 263.
[26] S. Block, J.A.H. Da Jornada, G.J. Piermarini, J. Am. Ceram. Soc. 68 (1985) 497.
[27] P. Bouvier G. Lucazeau, J.Raman Spectrosc., to be published.
[28] M.N. Rambert, thèse de doctorat, Bordeaux, 1997.
[29] G.J. Piermarini, S. Block, J.D. Barnett, R.A. Forman, J. Appl. Phys. 46 (1975) 2774.
[30] H. Arashi, M. Ishigame, Phys. State Solid 71 (1982) 313.
[31] G.A. Kourouklis, E. Liarokapis, J. Am. Ceram. Soc. 74 (1991) 520.
[32] D. Michel, M. Perez, Y. Jorba, R. Collongues, J. Raman Spectrosc. 5 (1976) 163.
[33] A. Feinberg, C.H. Perry, J. Phys. Chem. Solids 42 (1981) 513.
[34] R. Defay, I. Prigogine, Surface Tension, Adsorption, Wiley, New York, 1951.
[35] P. Desré, Philos. Mag. A 74 (1996) 103.
[36] P. Desré, NanoStructured Mater. 8 (1997) 687.
[37] P. Bouvier, E. Djurado, C. Ritter, A.J. Dianoux, G. Lucazeau, J. Inorg. Mater. 3 (2001) 647.

[38] O. Ohtaka, T. Yamanaka, S. Kume, E. Ito, A. Navrotsky, J. Am. Ceram. Soc. 74 (1991) 505.
[39] S. Kawasaki, T. Yamanaka, S. Kume, T. Ashida, J. Solid State Com. 76 (1990) 527.
[40] J.M. Leger, P.E. Tomaszewski, A. Atouf, A.S. Pereira, Phys. Rev. B 47 (1993) 14075.
[41] S. Desgreniers, K. Lagarec, Phys. Rev. B 59 (1999) 8467.
[42] P. Barberis, G. Corolleur-Thomas, R. Guinebretiere, T. Merle-Mejean, A.P. Mirgorodsky, P.E. Quintard, J. Nucl. Mater. 288 (2001) 241.
[43] H. Richter, Z.P. Wang, L. Ley, Solid State Commun. 39 (1981) 625.
[44] N. Petigny, P. Barberis, C. Lemaignan, Ch. Valot, M. Lallemant, J. Nucl. Mater. 280 (2000) 318.